Confinement and surface effects on the physical properties of rhombohedral-shape hematite (α-Fe_2O_3) nanocrystals

Carlos Luna[1,*], Aída D. Cuán-Guerra[1], Enrique D. Barriga-Castro[2], Nuria O. Núñez[3], Raquel Mendoza-Reséndez[1]

[1]Universidad Autónoma de Nuevo León (UANL), Av. Universidad S/N, San Nicolás de los Garza, Nuevo León 66450, Mexico.

[2]Centro de Investigación en Química Aplicada (CIQA), Blvd. Enrique Reyna Hermosillo No. 140, Saltillo, 25294 Coahuila, Mexico.

[3]Instituto de Ciencia de Materiales de Sevilla (ICMS), CSIC-US, Avda. Americo Vespucio n° 49, Isla de la Cartuja, 41092 Sevilla, Spain.

Correspondingauthor. *E-mail*: carlos.lunacd@uanl.edu.mx (C. Luna)

Abstract

The crystallization and physical properties of hematite (α-Fe_2O_3) nanocrystals with a rhombohedral shapeand with rounded edges,obtained by thermally induced hydrolysis of iron (III) solutions under acidic conditions and a fast nucleation,have beenrevisited in the present work. In particular, the morphological and themicrostructural properties of such nanocrystals have beeninvestigatedin detail as a function of aging time using severalcharacterization techniques, including X-ray diffraction, conventional and high

resolution transmission electron microscopyand selected area electron diffraction. Also different spectroscopies were employed to study the vibrational, optical and semiconductor properties of the obtained materials; concretely, studies of Fourier transform infrared and Raman spectroscopies confirmed the hematite phase of the rhombohedral nanocrystals, whose vibrational bands are shifted to lower frequencies relative to the bulk hematite onesas the aging time is reduced due to phonon confinement effects. Also, the indirect and direct transition band gaps were estimated from the UV-visible spectra using Tauc´s plot analysis, finding interesting dependences on the crystal size arising from quantum confinement and surface effects.

1. Introduction

The hydrolysis of iron (III) salt solutions thermally induced at temperatures around the boiling point, named forced hydrolysis,represents one of the more relevant route to obtain size- and shape-selected iron oxide nanomaterials due to its astonishing versatility.[1,2] In fact, the carefully exploration of this synthetic method during more than four decades ago, starting with pioneer investigations of Matijević, Ozaki, Ishikawa and other authors[3-6], has been crucial to investigate the crystallization phenomena in supersaturated solutions[7-10] and to study physical properties of the condensed matter at the nanoscale.[11-14]

Among thenanoscopic iron oxidesgrowth by forced hydrolysis, hematite (α-Fe_2O_3) nanostructures have received a special attention due to their variety of morphologies and sizes,[15-17]and their related optical,[18] magnetic[19,20] and photo-catalytic[21,22] properties,finding

a wide variety of practical applications.[21,23] In this regards, the great chemical stability of hematite and the vivid blood-red color of hematite become the colloidal α-Fe_2O_3particles valued pigments for paintings or to color glass and plastics.[18] Also, α-Fe_2O_3 materials are excellent UV absorbents.[24]In addition, very fine α-Fe_2O_3 nanocrystals exhibit interesting magnetic behaviors due to finite-size and surface effects, such as the dependence of the Morin transition on the particle size[25,26] and superparamagnetic and spin glass–like behaviors arising from the frustration of the antiferromagnetic coupling at the particle surface.[13]On the other hand, hematite is one of the cheapest semiconductor materialsthat exhibit a narrow band gap ($E_g \approx$ 2.2 eV) and a absorption of around the 40% of the solar spectrum energy.[27]On the other hand, hematite is one of the semiconductor materials less harmful to the environment.

α-Fe_2O_3 nanocrystals with few nanometers in size tends to self–assembly in solution into nanometric or submicrometric architectures with geometrical morphologies (such as spindles[17], cubes[28] or tubes[16])through oriented attachment processes.[29]The size and morphology of these attached nanocrystals and their self-assembly can be finely varied with the addition of surfactant agents,[30]modifying the hydrothermal conditions[8]and controlling the nucleation rate, the concentration of the iron salt and aging time.[31]The driving force of the oriented attachment of colloidal nanocrystals is the same as that of other crystal-growth mechanisms: a reduction of the crystal free energy leading to a decrease in surface energy, which is higher than the volumetric energy contribution.[10]On the other hand,as a consequence of the rhombohedral corundum-like crystal structure of hematite, colloidal α-

Fe_2O_3 nanocrystals obtained by the force hydrolysis of Fe^{3+} solutions and with dimensions around few tens of nanometers usually growths displaying rhombohedral shapes,[31,32]where the exposed faces are dependent on the pH of the reaction media, the presence of foreigner ions,[33]the nucleation rate and the ferric ions concentration,[31] among other parameters of synthesis.For instance, the α-Fe_2O_3 nanocrystals obtained by forced hydrolysis of acidic ferric chloride solutions tends to display {104} faces,[32,33] whereas the presence of perchlorate ions favored the formation of {102} faces.[33]The synthesis of these rhombohedral nanocrystals by forced hydrolysis typically takes several days,[32] however, the reaction time can be reduced with the addition of catalytic reagents such as urea,[10,34] or inducing a fast nucleation process by quickly pouring of the aqueous Fe^{3+}solution into boiling water under vigorous stirring.[31] In fact, a fast nucleation process impliesa direct transformation of amorphous iron oxides to crystalline hematite nanoparticles without the usual formation of intermediate phases (β-FeOOH or α-FeOOH[31]) commonly observed in forced hydrolysis of Fe^{3+} by slow nucleation processes.[31,35]

In the present contribution, the formation of rhombohedral-shape α-Fe_2O_3 nanocrystals by the forced hydrolysiswith a fast nucleation was revisited, and the evolution of the morphological, microstructural, optical and semiconductor properties of such nanocrystals were studied and correlated at different stages of the nanocrystal formation considering confinement and surface effects in their explanation.

2. Experimental Section

2.1. Chemicals

Anhydrous iron (III) chloride ($FeCl_3$, 97%, Sigma-Aldrich), hydrochloric acid (HCl, 37%, Sigma-Aldrich) and absolute ethanol were used without further purification. The water added in all experiments was doubly distilled.

2.2. Synthesis of samples

Hematite nanoparticles were prepared by forced hydrolysisin afast nucleation process following the procedure reported by Wang et al.[31] Concretely, 100 ml of an aqueous solution of $FeCl_3$ (0.01M, 0.8109g of $FeCl_3$) were mixed with 400 ml of boiling distilled water in presence of HCl (2mM) and under vigorous stirring. Afterwards, the mixture was aged at 98º C during a variable aging time, t_A: 0, 2, 8, 24, 30, 48, 50 and 56 h. The obtained colloidal particles were separated from their mother solution by centrifugation and washed several times with doubly distilled water and absolute ethanol. Lastly, a portion of the purified powder was re-dispersed in distilled water for further analysis of the samples in form of colloids, while the rest of the sample was dried in an oven at 50 °C for 5 h.

2.3. Characterization techniques

The samples if form of dried powder were studied by X-ray diffraction usingaX'pert Pro X-ray diffractometer (PANalitical) and Cu K_α radiation (λ =1.5418 Å).The mean coherence lengths, MCL_{hkl}, associated to the four more intense diffraction peaks of the samples were estimated from the full width at half maximum (FWHM) of the aforesaid peaks with the Scherrer equation:[36]

$$\mathrm{MCL}_{hkl} = \frac{0.9\,\lambda}{\beta\,\mathrm{Cos}\,\theta_B} \quad (1)$$

where λ is the X-ray wavelength, β is the broadening of the diffraction peak (after subtracting the instrumental broadening) and θ_B is the Bragg angle at which the maximum of the peak appears. The particle size, morphologyand crystalline structure of the samples were examined by transmission electron microscopy (TEM) using a FEI-TITAN 80-300kV microscope operated at 300 kV. For these analyses, conventional TEM, high-resolution transmission electron microscopy (HRTEM) and selected area electron diffraction (SAED) characterizations were employed using lacey carbon coated copper grids. The experimental data were recorded as digital images via a Gatan charge-coupled device (CCD) system and processed using Gatan´s Digital Micrograph software package. Ultraviolet-visible (UV-vis) absorption spectra in the wavelength range of 300-1100 nm were measured using a Thermo Scientific Evolution 60s UV-Vis spectrophotometer and bi-distilled water as reference and dispersive medium of samples. The indirect and direct transition band gaps, E_g, were estimated from Tauc´s plot analysis using the formula:

$$\alpha h\nu = A\left(h\nu - E_g\right)^n \quad (2)$$

whereα is the absorption coefficient, ν is the frequency of the photons, A is a constant and h is the Plank´s constant. The exponent n is equal to 0.5 for allowed direct transitions and 2 for allowed indirect transitions. Fourier Transform Infrared (FTIR) spectroscopy measurements were carried out using a Nicolet 510 Fourier Transform spectrometer that

was operated with the samples diluted in KBr pellets. Raman spectra were recorded with a Horiba HR800 UV Confocal Raman Microscope using a green laser (532.14nm) working at 600 line per mm, 100x objective, 20 mW and 0.1 mm pinhole.

3. Results and Discussion

Fig. 1 depicts XRD patterns of samples obtained at different aging time (t_A). For all samples, even for sample S-0h, well-defined diffraction peaks ascribed to a crystalline phase of hematite (Joint Committee on Powder Diffraction Standards file No. 33-0664, R-3C space group) are observed. Besides, in the case of samples obtained at aging time equal or below to 4 hours, additional broad peaks appear in the XRD patterns, whose relative intensities gradually vanish as t_A increases. These facts indicate that the fast nucleation process induced immediately the formation of hematite nanoparticles accompanied by the precipitation of amorphous or poorly crystallized iron oxide that tend to disappear ast_A increases. On the other hand, the relative intensities of the diffraction peaks of the hematite phase evolve as t_A is varied. In this manner, the relative intensity of the Bragg peak corresponding to the (104) planes increases as t_A increases. This observation suggests that the α-Fe_2O_3 nanocrystals predominantly exposed {104} crystal faces, feature that was more marked as the aging time was increased.

The crystal dimensions estimated from the Scherrer equation were also dependent on the aging time.Fig. 2 displays the mean coherence lengths perpendicular to different

hematite (hkl) planes, obtained using the equation (1). These data shownon-monotonous dependences that can be different in function of the studied (hkl) diffraction peaks.

Fig. 3 shows representative TEM images of samples obtained at different t_A. For the non-aged sample (i.e. S-0h), very fine nanoparticles or nuclei with average sizes of around 5 nm are formed, howeversome particles of this sample,in a minority proportion, displayed tens of nm (Fig. 3a). In agreement with the above mentioned XRD characterizations and the results reported by Wang et al.,[31] the finest nanoparticles could be amorphous or poorly crystallized iron oxide,and the particles of tens of nm in size could be associated to the early formation of hematite nanocrystals. As the aging time was increased, the presence of biggest particles significantly increased, and they acquiredrhombohedra-like morphologies (Fig. 3b-d), whereas the presence of the finest nanoparticles decreased until they practically disappeared at aging time above 8 hours, indicating that a crystal growth by Ostwald ripening occurs.[37,38] According to these remarks, the average particle size increased as t_A was increased up to 24 hours, and the mean particle size remainedalmost constant for longer aging time (Fig. 4b, c and d).

Figures 5a and 5c depict typical HRTEM images of α-Fe_2O_3 nanocrystals with rhombohedra shapes obtained at different aging time (4 and 24 hours, respectively). The indexation of the corresponding FFT images of these HRTEM images (see for example Fig. 5b) disclose that both nanocrystals are viewed along the [-441] direction with four side facets that correspond to {104} crystal planes.

These features are similar than those reported by Rodriguez et al.[32] for α-Fe_2O_3 nanocrystals with a rhombohedra shape obtainedthrough the forced hydrolysis of iron (III) chloride solutions but with a slow nucleation process. Therefore, the fast nucleation process accelerates the formation of the rhombohedral α-Fe_2O_3nanocrystals but not affect to their microstructural properties. Also, we can conclude that the rhombohedral crystals increases their size as t_A increases from 4h to 24 h, but their exposed faces don´t change. On the other hand, it is remarkable that we didn´t found the disk-like and tetrahedral-like hematite nanocrystal aggregates reported by Wang et al.[31] obtained under the fast nucleation process, probably because the formation of these supramolecular structures is strongly dependent on the solvent evaporation.[31]Interestingly, we observed in Fig. 5a and c that the edges of the long diagonal of both rhombohedra nanocrystals appear slightly rounded due to the occurrence of small exposed surfaces parallel to the crystal plane{110}.

The fact that the nanocrystals tend to appear as rhombohedra usually oriented along the [-441] direction suggests that these fine crystals tend to display a flattened morphology with the [-441] direction perpendicular to their flat surface. However, some additional particles apparently exhibit other polyhedral shapes.Wang et al. attributed this fact to the occurrence of a shape distribution of the particles,[31] however, the observation of several apparent morphologies is probably due to the nanocrystals can fall onto the TEM grid with different orientations. In this regards, Rodriguez et al. showed that a unique rhombohedral shape for α-Fe_2O_3 nanocrystals with {104} facets could explain the different apparent

particle shapes obtained through the forced hydrolysis of iron (III) chloride solutions with a slow nucleation,[32] which is consistent with more recent observations carried out by electron microscopy tomography.[39]Fig 6a shows a TEM micrograph of sample S-24h where several α-Fe_2O_3 nanocrystals are observed with different tilted positions into an open area of the lacey carbon film, confirming the model of Rodriguez et al.[32] Fig. 6b is the HRTEM of one of these particles. The indexation of its corresponding FFT pattern (Fig. 6c) indicated that this nanocrystal is observed in Figs. 6a and b along the [241] direction.Also, the TEM image of Fig. 6a shows that the α-Fe_2O_3nanocrystals usually present pores and fractures, in agreement with the formation of α-Fe_2O_3nanocrystals through the aggregation of poorly crystallized particles and coalescence proposed by Echigo et al.[39]Fig. 7 is a schematic representation of the formation mechanism of the rhombohedralα-Fe_2O_3nanocrystals with pores and fractures, consisting of the quick formation of amorphous or poorly crystallized nuclei, nuclei aggregation, coalescence, crystallization forming stable faces with pores, and finally, growth by Ostwald ripening.

Fig. 8 shows an example of the FTIR characterization of the rhombohedralα-Fe_2O_3 nanocrystals. Characteristic absorption peaks of hematite[40-42]appear at 470, 527, 576 and 645 cm^{-1}as very small bands in these spectra. We attributed the other peaks to material adsorbed on the nanocrystal surface from the reaction media. In fact, the wide and very intense peak observed at around 3420 cm^{-1} could be associated to the O-H vibration of physically absorbed water in the nanocrystals.[42] Also, the intense peak at 1606 cm^{-1} could be ascribed to the bending vibration of adsorbed water.[43] The abundance of OH groups and

physisorbedwater molecules is very usual in hematite nanoparticles prepared by hydrothermal and force hydrolysis methods.[44]

Fig. 9 shows the Raman spectrum of sample S-24h. The intense peaks at 221 and 280 cm^{-1} can be assigned to the A_{1g} and E_g Raman modes of the hematite phase.[40,45]These bands appear shifted to lower frequencies relative to the bulk hematite ones (226 and 292 cm^{-1})[40]due to phonon confinement effects arising from the nanoscopic size of the rhombohedral nanocrystals.[46]On the other hand, the weak and broad peaks at 386 and 586 cm^{-1} could be ascribed to the presence ofthe amorphous or poorly crystallized iron oxide nuclei.[31] Interestingly, an additional wide band is observed at around 1289 cm^{-1}. Owens et al. observed this band at 1295 cm^{-1} for a bulk hematite sample and shifted down to 1283 cm^{-1} for nanosized hematite,[46] and it was associated to the band reported by other authors at 1320 cm^{-1}.[47]This band has been frequently assigned to a two-magnon scattering arising from the antiferromagnetic nature of hematite,[47] however, several studies have shown that this band is actually due to a two-phonon mode,[46,48,49] falling the two-magnon scattering band at around 1525 cm^{-1}, which has been observed with Raman-scattering measurements carry out at different temperatures, high pressures and with isotopic oxygen substitution.[49]

The color of the colloidal suspensions of the nanocrystals was gradually changed from reddish brown to blood-red as the aging time was increased (see the insert of Fig. 10).To gain more information about the optical and semiconductor properties of samples, they were studied by UV-visible spectroscopy. Bulk stoichiometric hematite is a n-type

semiconductor whose valence band consists of full $2t_{2g}$ Fe 3d ligand field orbitals and a contribution of the oxygen antibonding 2p orbitals, whereas its conduction band is composed of empty Fe^{3+} 3d orbitals, being the band gap energy of bulk hematite around 2.2 eV.[40] Fig. 10 shows the UV-visible spectra of samples obtained at different aging time. Such spectra indicated that all samples show strong absorption of electromagnetic radiation in the UV region and to a lesser extent in the violet-blue region, which could be ascribed to two kinds of electronic transitions: the absorption in the UV range related to the directcharge transition of O^{2-} 2p$\rightarrow$$Fe^{3+}$ 3d, and the absorption in the violet-blue range related to the indirect charge transition $2Fe^{3+} \rightarrow Fe^{2+} + Fe^{4+}$.[18,27]Interestingly, the absorption curves tend to experience a shift to higher frequencies (smaller wavelengths) as the aging time decreases. This *blue shift* is associated to the reduction of the nanocrystal size, as it has been observed in other semiconductor systems.[50]For the non-aged sample (t_A = 0h), the absorbance continuously decreased as the wavelength decreased in the wavelength range from 300 to 1,000 nm. However, for aged samples at 98º C, the absorbance exhibiteda peak and a shoulder, which we named K_1 and K_2, respectively, and that both experienced a shift from 362 and 525 nm to 390 and 540 nmas the aging time was increased from 8 to 56 hours, respectively.

TheTauc´s plot analysis (see illustrative examples in Fig. 11a and b) indicated that the indirect a direct transition band gap energies decreased from 2.43 and 2.79 to 1.91 and 2.18 eV as t_A increased (Fig 10c and d), respectively, being the values of the band gaps at the largest aging time very close to values reported for bulk hematite,[27] and around 25% larger than the bulk values at t_A =4h. These dependences are attributed to the dependence of

the dimensions of the nanocrystals on the aging time and the increasing contribution of the quantum confinement and surface effects as the crystal size is decreased to few nm. As Fondell et al. have recently shown,[51]the quantum confinement effects significantly affects to the optical properties of low dimensional hematite with dimensions below 20 nm. On the other hand, stoichiometric deviations are expected at the nanocrystal surface due to its reduced coordination number, roughness and the presence ofpores, which should have a notorious effect on the semiconductor properties when the surface / volume ratio of the nanocrystals is enough large.

Conclusions

Hematite nanosizedcrystals with rhombohedral morphologies have been prepared by forced hydrolysis in a fast nucleation process. The formation mechanism of these crystals occurs by a fast nucleation of very fine amorphous iron oxide nanoparticles that grow firstly by aggregation and coalescence,and then by Ostwald ripening forming hematite nanocrystals with a rhombohedral morphology. The resulting rhombohedral nanocrystals are composed of four {104} side facets, two {110} faces at the edges of the long diagonal of the nanocrystals and two {-441} facets as the top and bottom faces. These crystals have vibrational properties with resonant frequencies shifted to lower frequencies relative to the bulk hematite onesdue to phonon confinement effects. Also, these nanoscopic crystals exhibitstrong absorption of electromagnetic radiation in the UV region and a lesser extent in the violet-blue region that experience a shift to higher frequencies as their sizes are decreased, exhibitingindirect a direct transition band gap energies that can be up to 25% larger than the bulk values due to quantum confinement and surface effects.

Acknowledgements

Financial support from the *Mexican Secretariat of Public Education / Sub-Secretaría de EducaciónPublica* (SEP-PROMEP), the *Mexican Council of Science and Technology / ConsejoNacional de Ciencia y Tecnología* (CONACYT), and Universidad Autónoma de Nuevo León (UANL) under research projects "*Redestematicas de colaboración*","*CB-179486*" and "*PAICYT*", respectively, is acknowledged.

References

[1] Bailey, J. K.; Brinker, C. J.;Mecartney, M. L. Growth mechanisms of iron oxide particles of differing morphologies from the forced hydrolysis of ferric chloride solutions. *Journal of Colloid and Interface Science***1993**, *157*, 1-13.

[2] Kandori, K.; Yamamoto, N.; Yasukawa, A.; Ishikawa, T. Preparation and characterization of disk-shaped hematite particles by a forced hydrolysis reaction in the presence of polyvinyl alcohol. *Physical Chemistry Chemical Physics***2002**, *4*, 6116-6122.

[3] Matijević, E.; Scheiner, P. Ferrichydrous oxide sols: III. Preparation of uniformparticlesbyhydrolysis of Fe (III)-chloride,-nitrate, and-perchloratesolutions. *Journal of Colloid and Interface Science*, **1978**, *63*, 509-524.

[4] Hamada, S.; Matijević, E. Formation of monodispersedcolloidalcubichaematiteparticles in etanol + watersolutions. *Journal of theChemicalSociety, Faraday Transactions 1: PhysicalChemistry in Condensed Phases*, **1982**, *78*, 2147-2156.

[5] Ozaki, M.; Matijević, E. Preparation and magneticproperties of monodispersedspindle-type γ-Fe_2O_3particles. *Journal of colloid and interface science*, **1985**, *107*, 199-203.

[6] Ishikawa, T.; Matijevic, E. Formation of monodispersedpure and coatedspindle-typeironparticles. *Langmuir*, **1988**, *4*, 26-31.

[7] Ocaña, M.; Morales, M. P.; Serna, C. J.The growth mechanism of α-Fe2O3 ellipsoidal particles in solution.*Journal of colloid and interface science***1995**, *171*, 85-91.

[8] Jia, C. J.; Sun, L. D.; Yan, Z. G.; Pang, Y. C.; You, L. P.; Yan, C. H. Iron oxide tube-in-tube nanostructures. *The Journal of Physical Chemistry C***2007**, *111*, 13022-13027.

[9] Cai, J.; Chen, S.; Ji, M.; Hu, J.; Ma, Y.; Qi, L. Organic additive-free synthesis of mesocrystalline hematite nanoplates via two-dimensional oriented attachment. *CrystEngComm*, **2014**,*16*, 1553-1559.

[10] Luna, C.; Barriga-Castro, E. D.; Mendoza-Reséndez, R. The effects of aging time on the size, morphology, oriented attachment and magnetic behavior of hematite nanocrystals synthesized by forced hydrolysis of Fe III solutions. *ActaMaterialia*, **2014**,*66*, 405-413.

[11] McCarty, K. F. Inelastic light scattering in α-Fe_2O_3: Phonon vsmagnon scattering. *Solid state communications*, **1988**, *68*, 799-802.

[12] Wong, S. S.; Brus, L. E. Narrow Mie optical cavity resonances from individual 100 nm hematite crystallites. *The Journal of Physical Chemistry B*, **2001**, *105*, 599-603.

[13] Luna, C.; Vega, V.; Prida, V. M.; Mendoza-Reséndez, R. Morin Transition in Hematite Nanocrystals Self-Assembled Into Three-Dimensional Structures.*Journal of nanoscience and nanotechnology*, **2012**, *12*, 7571-7576.

[14] Luna, C.; Ilyn, M.; Vega, V.; Prida, V. M.; González, J.; Mendoza-Reséndez, R.Sizedistribution and frustratedantiferromagneticcouplingeffectsonthemagneticbehavior of

ultrafineakaganéite (β-FeOOH) nanoparticles. *TheJournal of PhysicalChemistry C*, **2014**, *118*, 21128-21139.

[15] Jia, C. J.; Sun, L. D.; Yan, Z. G.; You, L. P.; Luo, F.; Han, X. D.; et al. Single- Crystalline Iron Oxide Nanotubes. *AngewandteChemie*, **2005**, *117*, 4402-4407.

[16] Xiong, Y.; Li, Z.; Li, X.; Hu, B.; Xie, Y. Thermallystablehematitehollownanowires. *Inorganicchemistry*, **2004**, *43*, 6540-6542.

[17] Mendoza-Reséndez, R.; Luna, C.; Barriga-Castro, E. D.; Bonville, P.; Serna, C. J.Control of crystallite orientation and size in Fe and FeConanoneedles.*Nanotechnology*, **2012**, *23*, 225601.

[18] Cao, R. B.; Chen, X. Q.; Shen, W. H.; Long, Z. A facile route to synthesize nano-hematite colloid.*Materials Letters*, **2011**, *65*, 3298-3300.

[19]Morin, F. J.Magnetic Susceptibility of α-Fe_2O_3 and α-Fe_2O_3 with Added Titanium*Phys. Rev.***1950**, *78*, 819-820.

[20] Zysler, R. D.; Fiorani, D.; Testa, A. M. Investigation of magnetic properties of interacting Fe 2 O 3 nanoparticles.*Journal of magnetism and magnetic materials*, **2001**, *224*, 5-11.

[21] Zeng, S.; Tang, K.; Li, T.; Liang, Z.; Wang, D.; Wang, Y.; et al. Facile route for the fabrication of porous hematite nanoflowers: its synthesis, growth mechanism, application in the lithium ion battery, and magnetic and photocatalytic properties. *The Journal of Physical Chemistry C*, **2008**, *112*, 4836-4843.

[22] Chen, Y. H.; Li, F. A. Kinetic study on removal of copper (II) using goethite and hematite nano-photocatalysts.*Journal of Colloid and Interface Science*, **2010**, *347*, 277-281.

[23] Li, L.; Koshizaki, N. Vertically aligned and ordered hematite hierarchical columnar arrays for applications in field-emission, superhydrophilicity, and photocatalysis. *Journal of Materials Chemistry***2010**, *20*, 2972-2978.

[24] Buxbaum G.; Pfaff G. Industrial Inorganic Pigment. Weinheim: VCH. 2005. p. 265.

[25]Amin, N.;Arajs, S. Morin temperature of annealed submicronic α-Fe_2O_3 particles.*Physical Review B***1987**,*35*, 4810-4811.

[26] Wu, C., Yin, P., Zhu, X., OuYang, C., &Xie, Y. Synthesis of hematite (α-Fe2O3) nanorods: diameter-size and shape effects on their applications in magnetism, lithium ion battery, and gas sensors. *The Journal of Physical Chemistry B*,**2006**, *110*, 17806-17812.

[27] Zhang, Z.; Hossain, M. F.; Takahashi, T. Self-assembled hematite (α-Fe_2O_3) nanotube arrays for photoelectrocatalytic degradation of azo dye under simulated solar light irradiation. *Applied Catalysis B: Environmental***2010**, *95*, 423-429.

[28] Chen, J. S.; Zhu, T.; Li, C. M.; Lou, X. W. Building hematite nanostructures by oriented attachment. *AngewandteChemie International Edition*, **2011**, *50*, 650-653.

[29] Niederberger, M., &Cölfen, H. (2006). Oriented attachment and mesocrystals: non-classical crystallization mechanisms based on nanoparticle assembly. *Physical Chemistry Chemical Physics*, *8*(28), 3271-3287.

[30]Kandori, K.; Hayashi, K.; Matsukawa, M.; Fukusumi, M.; Morisada, Y. Effects of Pluronics surfactants on morphology and porosity of hematite particles produced from forced hydrolysis reaction. *Colloid and Polymer Science*,**2010**,*288*(10-11), 1071-1079.

[31] Wang, W.; Howe, J. Y.; Gu, B. Structure and morphology evolution of hematite (α-Fe2O3) nanoparticles in forced hydrolysis of ferric chloride.*The Journal of Physical Chemistry C***2008**, *112*(25), 9203-9208.

[32] Rodriguez, R. D.; Demaille, D.; Lacaze, E.; Jupille, J.; Chaneac, C.; Jolivet, J. P. Rhombohedralshape of hematitenanocrystalssynthesizedviathermolysis of anadditive-free ferricchloridesolution. *TheJournal of PhysicalChemistry C***2007**, *111*(45), 16866-16870.

[33] Reeves, N. J.; Mann, S. Influence of inorganic and organic additives on the tailored synthesis of iron oxides. *J. Chem. Soc., Faraday Trans.*, **1991**, *87*, 3875-3880.

[34] Ocaña, M.; Morales, M. P.; Serna, C. J. Homogeneous precipitation of uniform α-Fe $_2O_3$ particles from iron salts solutions in the presence of urea. *Journal of colloid and interface science***1999**, *212*(2), 317-323.

[35] Gotić, M.; Popović, S.; Ljubešić, N.; Musić, S. Structural properties of precipitates formed by hydrolysis of Fe3+ ions in aqueous solutions containing NO 3− and Cl− ions. *Journal of materials science***1994**, *29*, 2474-2480.

[36] Cullity, B. D.; Stock, S. R. *Elements of X-rayDiffraction*.**2001.**UpperSaddleRiver, NJ: Prentice hall.

[37] Yao, J. H.; Elder, K. R.; Guo, H.; Grant, M. Theory and simulation of Ostwald ripening. *Physical review B***1993**, *47*, 14110.

[38] Luna, C.; Chávez, V. H. G.; Barriga-Castro, E. D.; Núñez, N. O.; Mendoza-Reséndez, R. Biosynthesis of silver fine particles and particles decorated with nanoparticles using the extract of Illiciumverum (star anise) seeds. *SpectrochimicaActa Part A: Molecular and Biomolecular Spectroscopy***2015** ,*141*, 43-50.

[39] Echigo, T.; Monsegue, N.; Aruguete, D. M.; Murayama, M.; Hochella, M. F. Nanopores in hematite (α-Fe2O3) nanocrystalsobservedbyelectrontomography. *American Mineralogist***2013**, *98*, 154-162.

[40] Cornell, R. M.; Schertmann, U.*The Iron Oxides*, 2nd Ed; Wiley-VCH: Weinheim 2003.

[41] Serna, C. J.; Rendon, J. L.; Iglesias, J. E. Infrared surface modes in corundum-type microcrystalline oxides. *SpectrochimicaActa Part A: Molecular Spectroscopy*, **1982**, *38*, 797-802.

[42] Lu, J.; Peng, Q.; Wang, Z.; Nan, C.; Li, L.; Li, Y. Hematite nanodiscs exposing (001) facets: synthesis, formation mechanism and application for Li-ion batteries. *Journal of Materials Chemistry A***2013**,*1*, 5232-5237.

[43] Wang, W.; Liang, L.; Johs, A.; Gu, B. Thin films of uniform hematite nanoparticles: control of surface hydrophobicity and self-assembly. *Journal of Materials Chemistry***2008**, *18*, 5770-5775.

[44]Jing, Z.; Wu, S. Synthesis and characterization of monodisperse hematite nanoparticles modified by surfactants via hydrothermal approach.*Materials Letters***2004** ,*58*, 3637-3640.

[45] Gou, X.; Wang, G.; Park, J.; Liu, H.; Yang, J. Monodisperse hematite porous nanospheres: synthesis, characterization, and applications for gas sensors. *Nanotechnology***2008**, *19*, 125606.

[46] Owens, F. J.; Orosz, J. Effect of nanosizing on lattice and magnon modes of hematite. *Solid State Communications* **2006**, *138*(2), 95-98.

[47] De Faria D. L. A.; Venâncio Silva, S.; De Oliveira, M. T. Raman microspectroscopy of some iron oxides and oxyhydroxides.*Journal of Raman spectroscopy***1997**, *28*, 873-878.

[48] McCarty, K. F. Inelastic light scattering in α-Fe_2O_3: Phonon vsmagnon scattering. *Solid state communications***1988** ,*68*, 799-802.

[49] Massey, M. J.; Baier, U.; Merlin, R.; Weber, W. H. Effects of pressure and isotopic substitution on the Raman spectrum of α-Fe_2O_3: Identification of two-magnon scattering. *Physical Review B***1990**, *41*, 7822.

[50] Zeng, S.; Tang, K.; Li, T. Controlled synthesis of α-Fe_2O_3nanorods and its size-dependent optical absorption, electrochemical, and magnetic properties. *Journal of colloid and interface science***2007**, *312*, 513-521.

[51] Fondell, M.; Jacobsson, T. J.; Boman, M.; Edvinsson, T. Optical quantum confinement in low dimensional hematite.*Journal of Materials Chemistry A***2014**, *2*, 3352-3363.

Figures

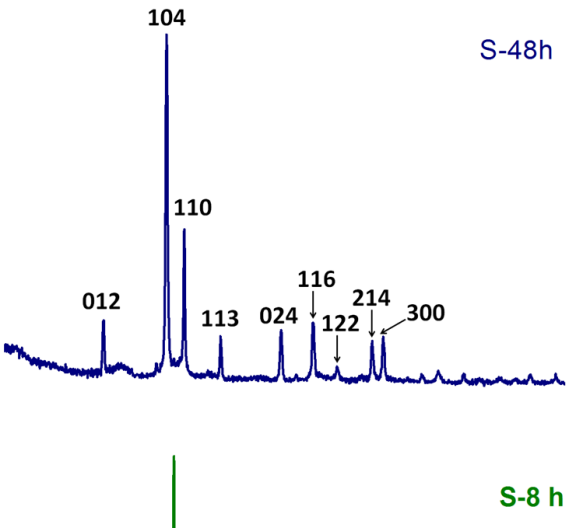

Fig. 1. XRD patterns of hematite samples obtained at different aging time.

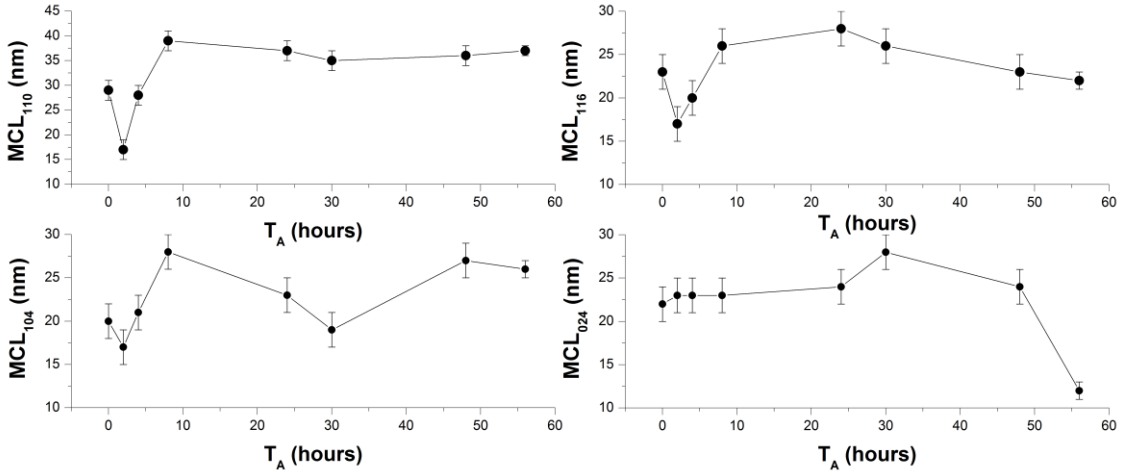

Fig. 2. Mean coherence lengths perpendicular to (110), (104), (116) and (024) crystallographic planes, respectively

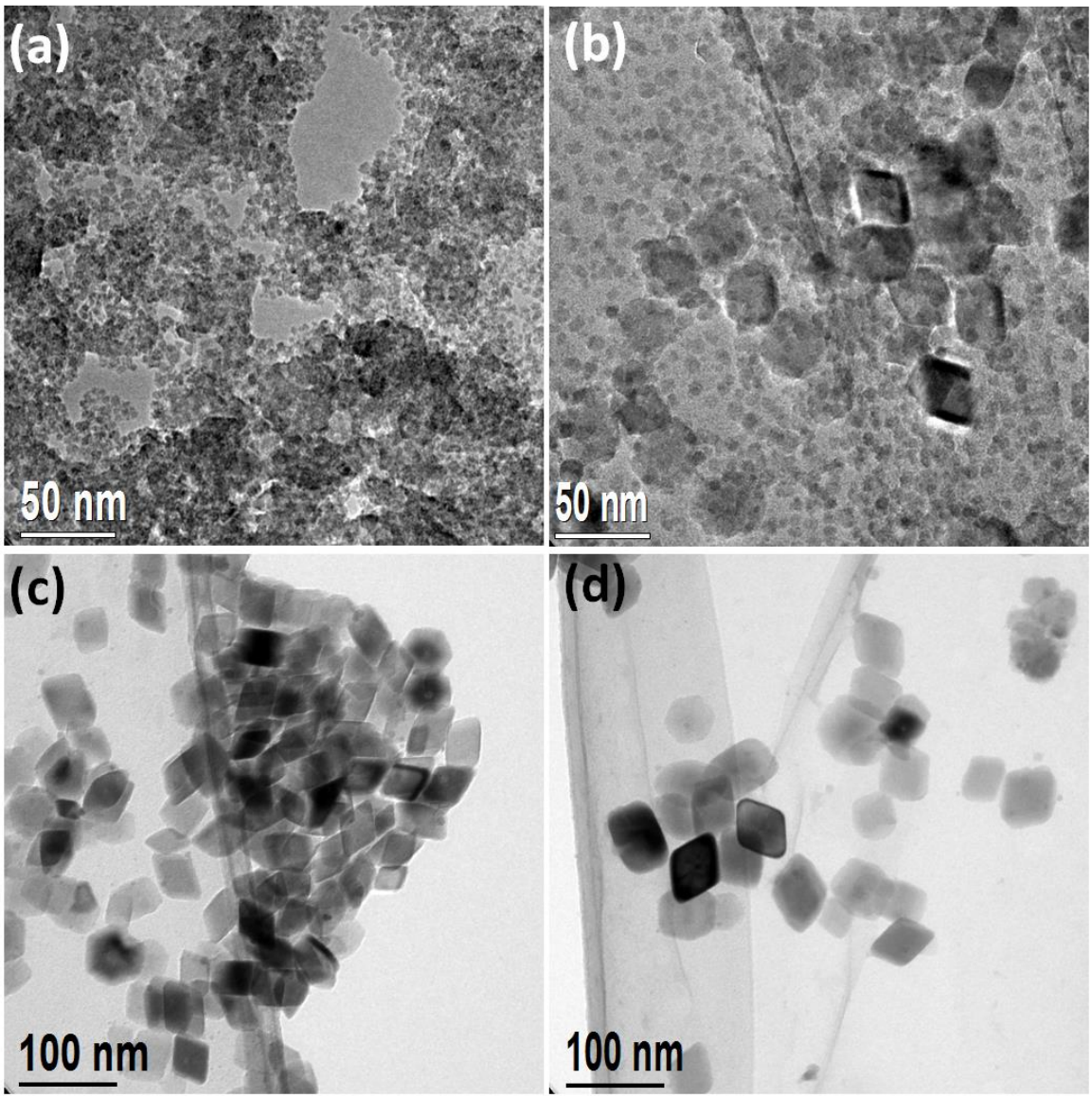

Fig. 3. TEM images of samples a) S-0h, b) S-4h, c) S-28h and d) S-48h.

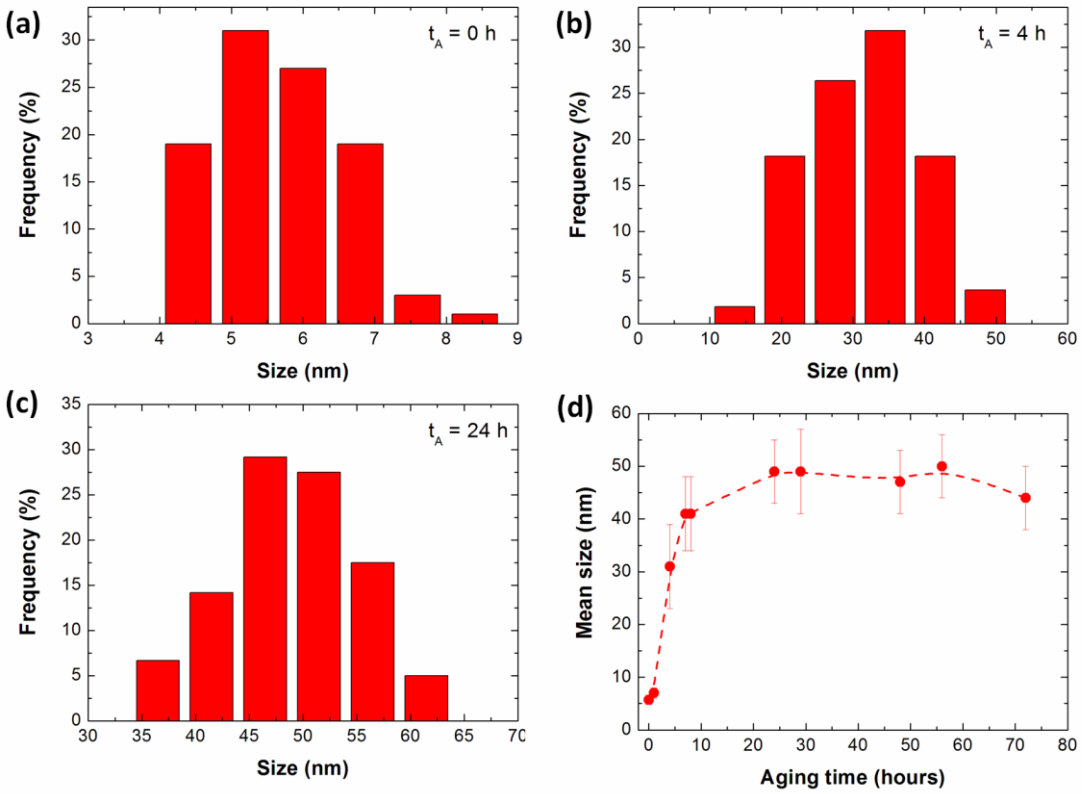

Fig. 4. Particle size distributions of samples a) S-0h, b) S-4h and c) S-24h. d) Mean size of the nanoparticles as a function of the aging time.

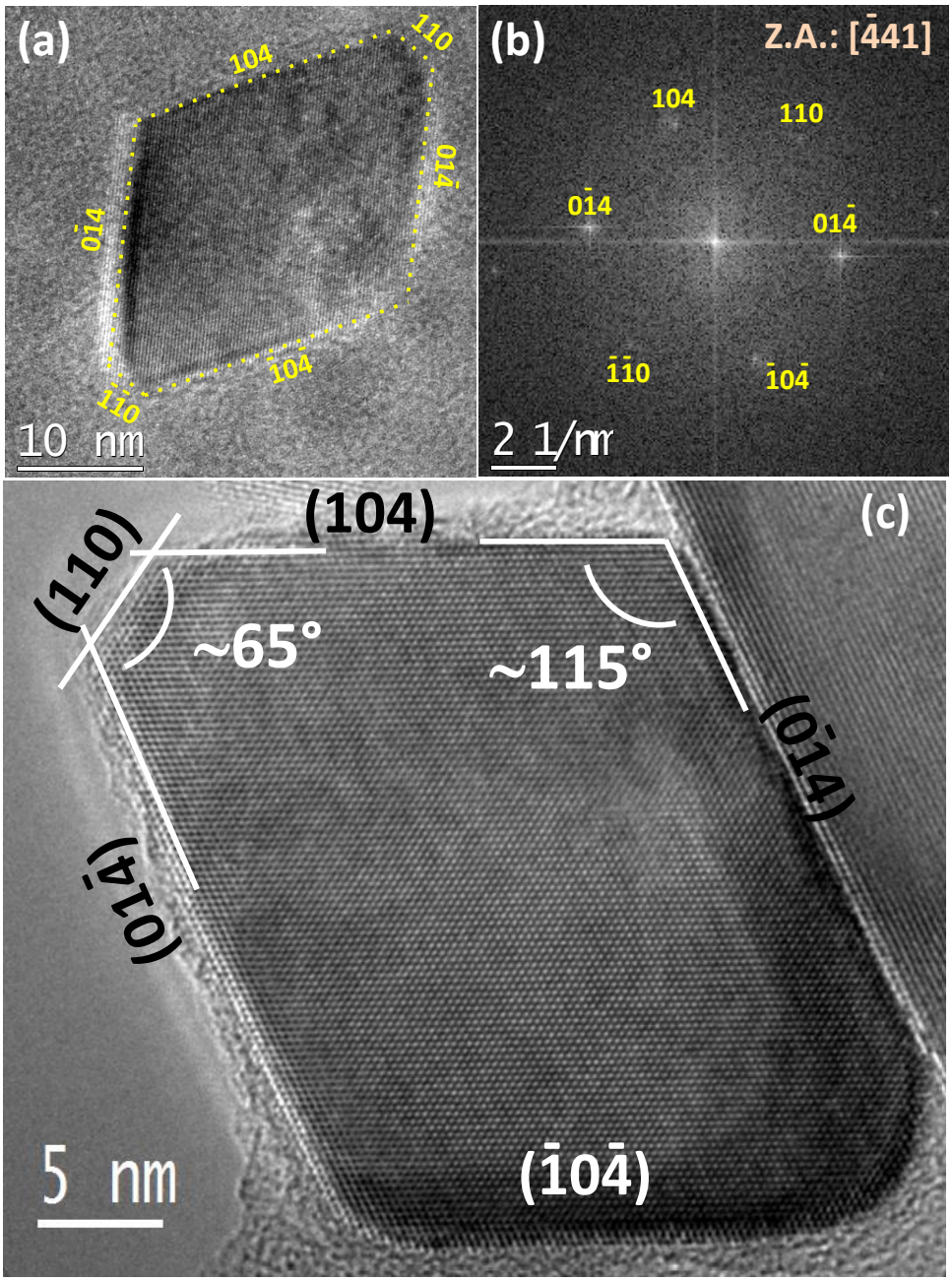

Fig. 5. HRTEM images of rhombohedral-shape hematite nanocrystals of samples a) S-4h and c) S-24h. Both crystals are viewed along the direction [-441] and present the same crystal facets. b) Fast Fourier Transform (FFT) pattern corresponding to image a) indexed to the [-441] zone axis of the hematite structure.

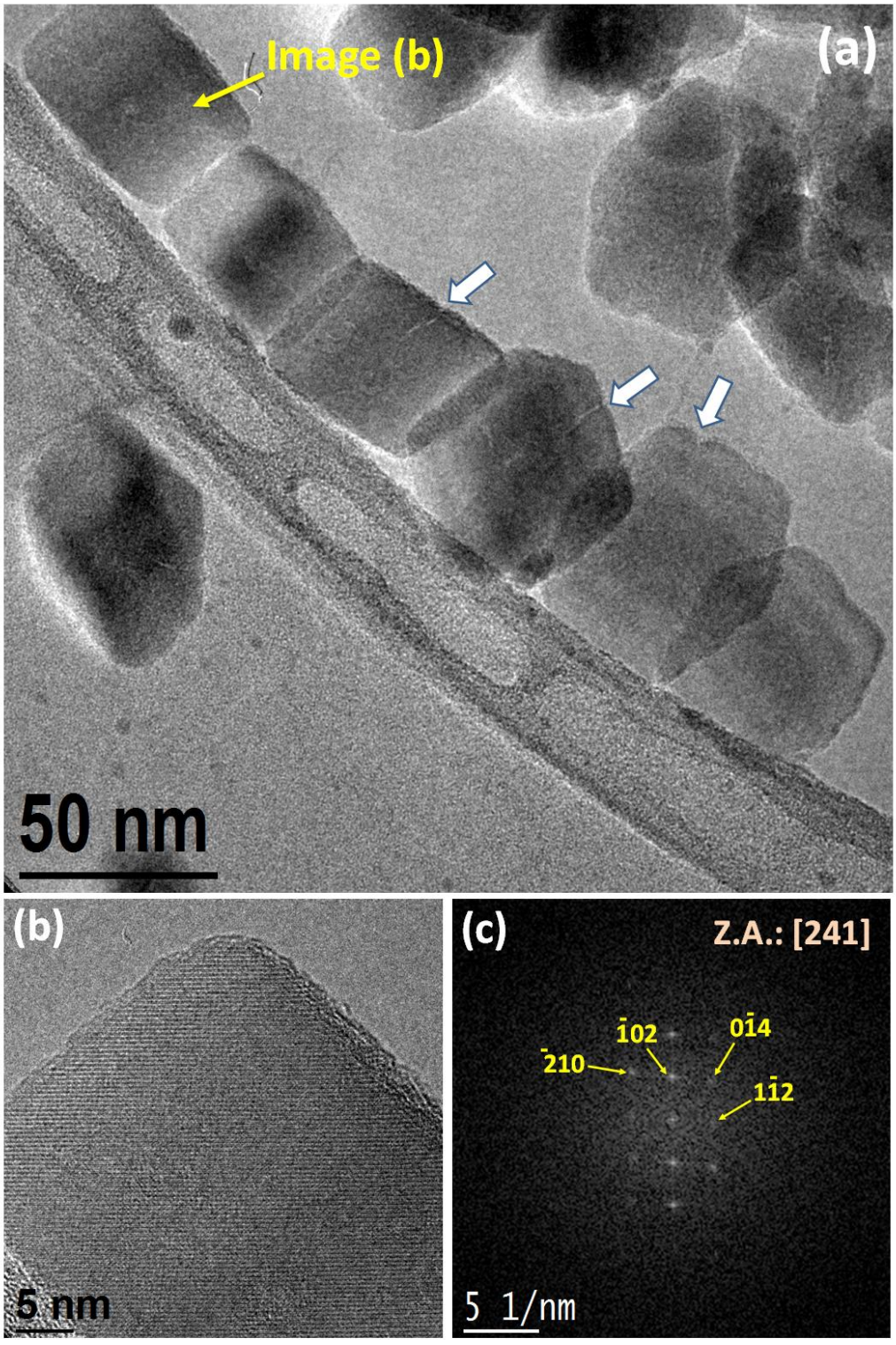

Fig. 6. a) TEM image of sample S-24h where several α-Fe_2O_3 nanocrystals are observed with different orientations. b) HRTEM of the nanocrystal highlighted in the panel a) by a yellow arrow.White arrows highlight some pores of the nanocrystals. c) FFT pattern corresponding to panel b) indexed to the [241] axis zone of the hematite structure.

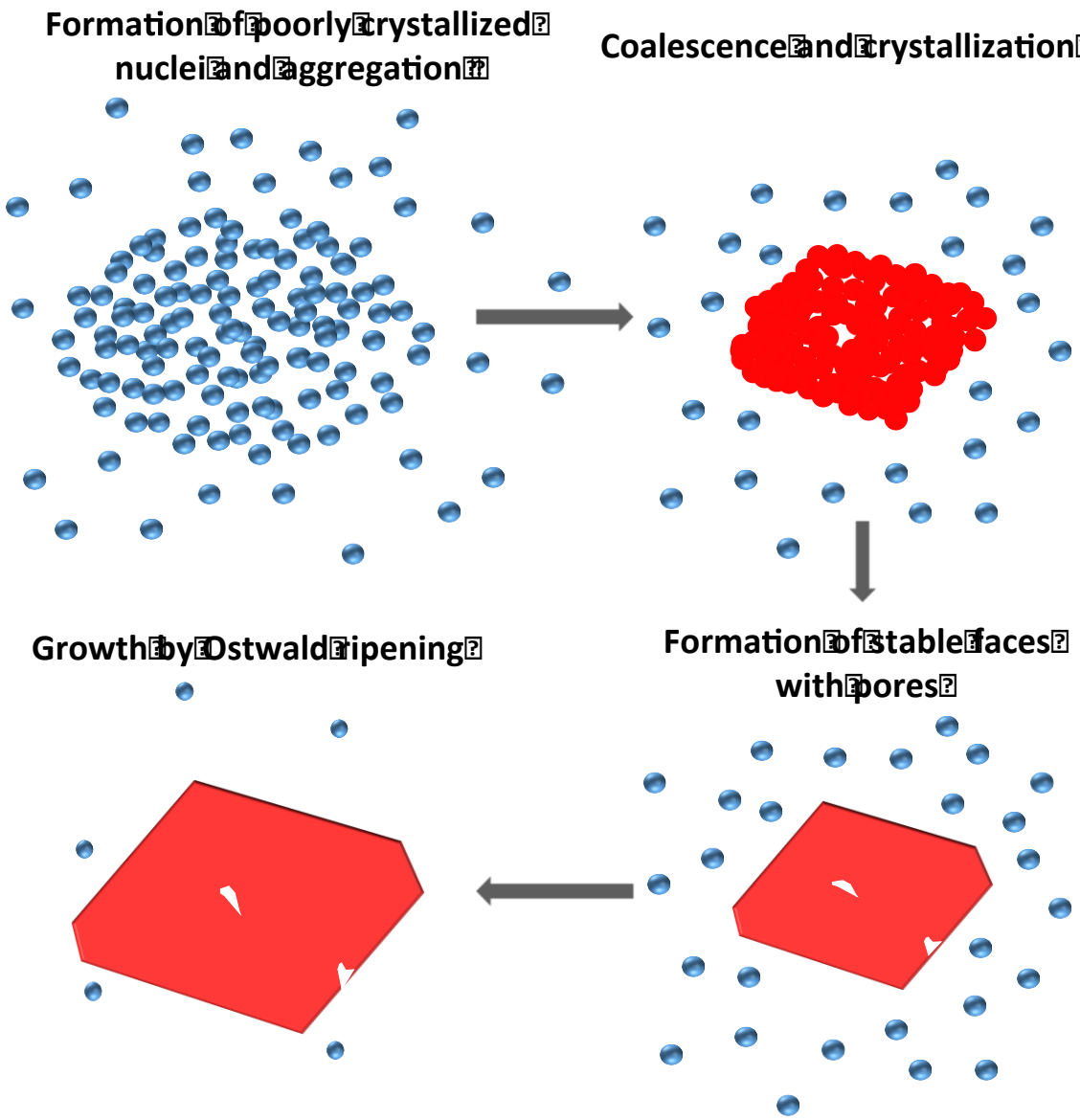

Fig. 7. Schematic representation of the formation mechanism of the rhombohedral hematite nanocrystals.

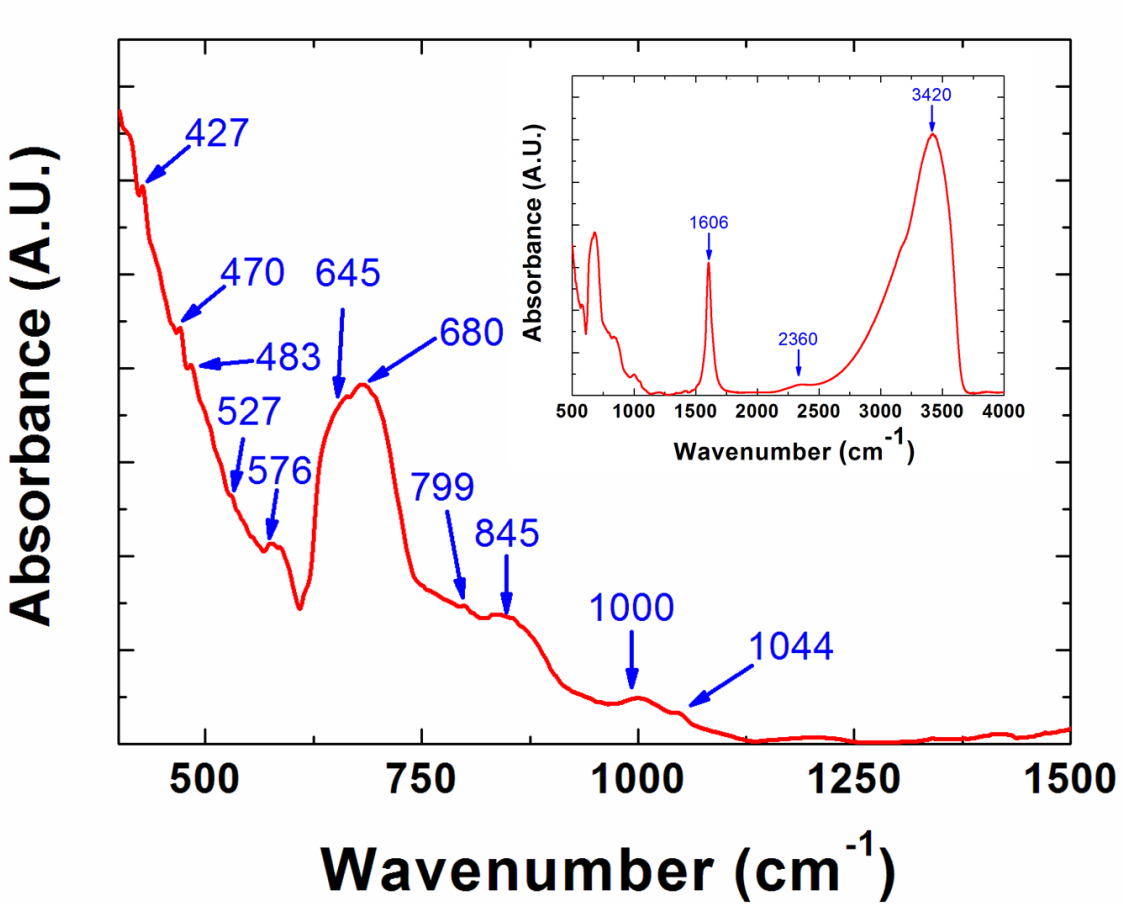

Fig. 8. Infrared spectrum of the sample S-24h

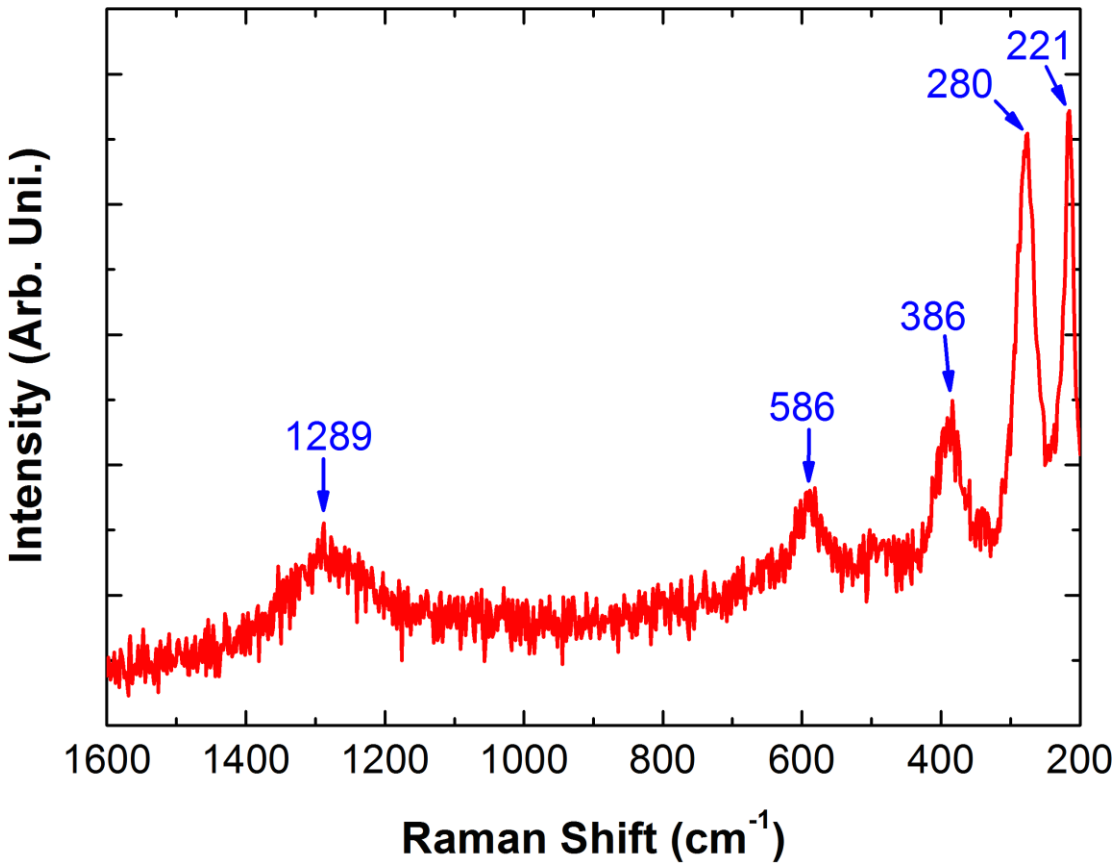

Fig. 9. Raman spectrum of the sample S-24h.

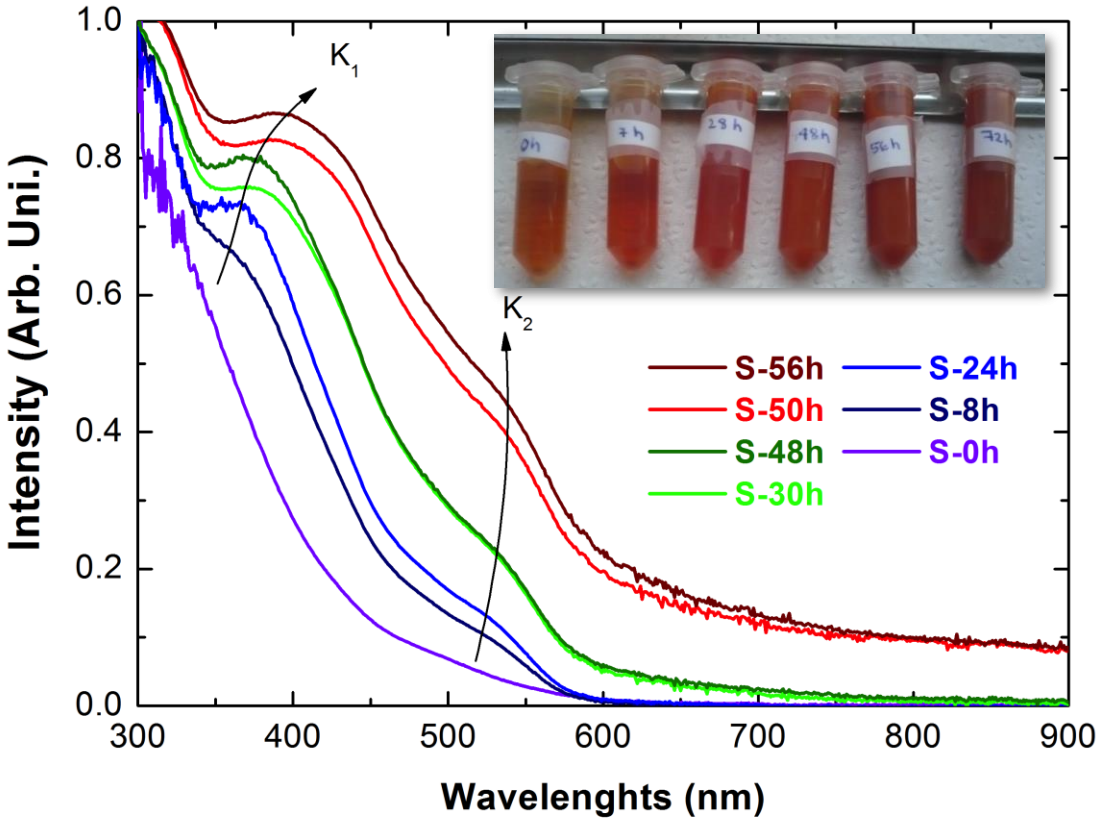

Fig. 10. UV-visible spectra of samples obtained at different aging time. The spectra of samples obtained at t_A equal or above 8 h exhibits a peak K_1 in the ultraviolet region and a shoulder K_2 in the visible region. The insert is a photograph of colloids of hematite nanocrystals obtained at different aging time.

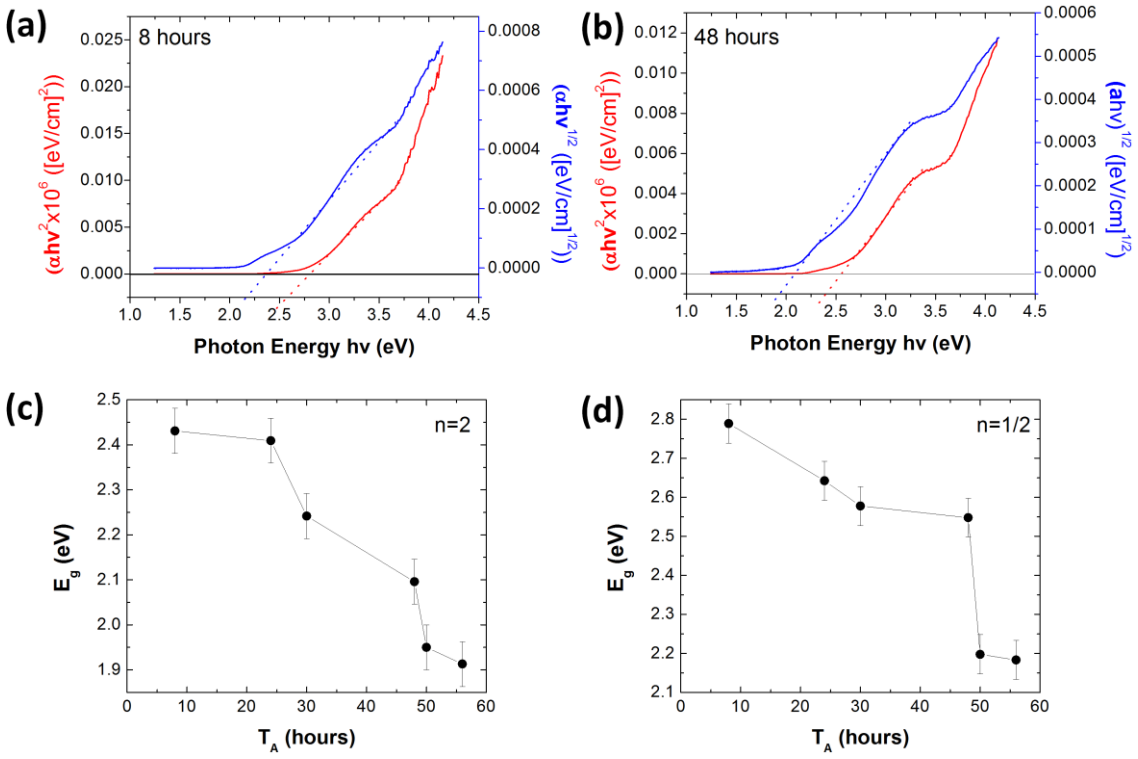

Fig. 11. Tauc´s plot analysis for samples a) S-8h and b) S-48h. Panels c) and d) represent the dependences of the indirect a direct transition band gap energies obtained from the Tauc´s plot analysis on the aging time, respectively.